ELSEVIER

Biophysical Chemistry 69 (1997) 269–281

Biophysical Chemistry

Channels formed by the transmembrane helix of phospholamban: a simulation study

Mark S.P. Sansom [a,*], Graham R. Smith [a], Oliver S. Smart [b], Steven O. Smith [c]

[a] *Laboratory of Molecular Biophysics, The Rex Richards Building, University of Oxford, South Parks Road, Oxford, OX1 3QU, UK*
[b] *Department of Crystallography, Birkbeck College, University of London, Malet Street, London, WC1 7HX, UK*
[c] *Department of Molecular Biophysics and Biochemistry, Yale University, 266 Whitney Avenue, PO Box 208114, New Haven, CT 06520-8114, USA*

Received 5 June 1997; revised 28 August 1997; accepted 28 August 1997

Abstract

Phospholamban is a small membrane protein which can form cation selective ion channels in lipid bilayers. Each subunit contains a single, largely hydrophobic transmembrane helix. The helices are thought to assemble as a pentameric and approximately parallel bundle surrounding a central pore. A model of this assembly (PDB code 1PSL) has been used as the starting point for molecular dynamics (MD) simulations of a system consisting of the pentameric helix bundle, plus 217 water molecules located within and at either mouth of the pore. Interhelix distance restraints were employed to maintain the integrity of the helix bundle during a 500 ps MD simulation. Water molecules within the pore exhibited reduced diffusional and rotational mobility. Interactions between the α-helix dipoles and the water dipoles, the latter aligned anti-parallel to the former, contribute to the stability of the system. Analysis of the potential energy of interaction of a K^+ ion as it was moved through the pore suggested that unfavourable interactions of the cation with the aligned helix dipoles at the N-terminal mouth were overcome by favourable ion–water interactions. Comparable analysis for a Cl ion revealed that the ion–(pore + water) interactions were unfavourable along the whole of the pore, increasingly so from the N- to the C-terminal mouth. Overall, the interaction energy profiles were consistent with a pore selective for cations over anions. Pore radius profiles were used to predict a channel conductance of 50 to 70 ps in 0.2 M KCl, which compares well with an experimental value of 100 ps. © 1997 Elsevier Science B.V.

Keywords: Phospholamban; Transmembrane helix; Channel conductance

1. Introduction

Ion channels are integral membrane proteins which allow otherwise impermeable ions to cross biological membranes at close to diffusion limited rates (ca. 10^7 ions/s) [1]. They achieve this by forming water-filled pores in membranes through which selected ions pass. Molecular dynamics simulations provide a tool for exploring the nature of the interactions between ion and channel during permeation. To date, most simulation studies on ion channels have been concerned with channel-forming peptides [2–5] or with simplified models of more complex channels

* Corresponding author. Tel.: +44-1865-275371; fax: +44-1865-510454; e-mail: mark@biop.ox.ac.uk

PII S0301-4622(97)00109-9

[6,7]. However, a problem with extending such studies channel proteins per se is the paucity of structural information for such proteins. A valuable next step is to analyze the behaviour of water within channels formed by relatively 'simple' membrane proteins, of which two of the best characterized examples are phospholamban (from cardiac sarcoplasmic reticulum; [8–11]) and the M2 protein of influenza A virus [12–14]. Both of these proteins contain only a single transmembrane (TM) helix within each subunit. These assemble to form a bundle of five (phospholamban) or four (flu M2) parallel helices within the membrane.

The structure of the phospholamban helix bundle has been characterised by a combination of mutagenesis, spectroscopic and computational techniques [9,10,15–17]. The polypeptide chain is 52 residues in length. Residues 35–52 form a single hydrophobic TM helix (although it has been suggested that somewhat longer helices, from 26–52 may be involved; [17]), and five such helices form a parallel, left-handed supercoil within the membrane, surrounding a central pore [10,11]. There is a debate concerning the in vivo role of phospholamban in the cardiac sarcoplasmic reticulum [18,19]. In particular it is argued whether channel activity [11] or direct protein–protein interactions [20,21] are responsible for the negative regulatory action of phospholamban on the Ca^{2+} pump. However, when reconstituted in lipid bilayers phospholamban does form ion channels [8]. The channels formed by phospholamban are permeable to Ca^{2+} and to K^+ ions. Channels may also be formed by assemblies of synthetic peptides corresponding to just the TM domains of phospholamban, although such channels may differ subtly from those formed by the intact protein [8,11]. Thus, to some extent regardless of the physiological role of such channels, one is left with the biophysical problem of the nature of a channel formed by a bundle of hydrophobic α-helices which lack any polar, pore-lining sidechains. It is this problem which this paper sets out to explore, from an MD simulation perspective.

In this paper a model of the phospholamban pore, derived from conformational searching and in vacuo restrained molecular dynamics (MD) simulations by Adams et al. [10], is the starting point of MD simulations of a water-filled phospholamban TM helix bundle. The properties of intra-pore water and their contributions to the energetics of the helix bundle are analyzed. The energetics of a K^+ ion and of a Cl^- ion translated along the pore are determined, and the pore radius profile is used to predict the conductance of the pore, enabling comparison with experimental data.

2. Methods

2.1. General

MD simulations were performed using CHARMm [22] version 23f3. The parameter set employed was version 22, with only polar H atoms represented explicitly. This was modified so as to treat the Hγ atom of Cys sidechains as an explicit (i.e., polar) hydrogen. Simulations were run on a DEC 2100 4/275. All other calculations were on Silicon Graphics R4000 workstations. Structures were visualized using Quanta V4.0 (Biosym/Molecular Simulations), and diagrams were drawn using Quanta or Molscript [23].

2.2. MD simulations of a solvated phospholamban pore

The initial model of a phospholamban pore was extracted from the Brookhaven database [24] (code 1PSL). This is the model described by Adams et al. [10] and Arkin et al. [11], containing non-hydrogen atoms only. Polar hydrogen atoms were added to the structure using the molecular editor in Quanta. The termini of the helices were such that the N-termini were free and unprotonated, whilst the C-termini were free and negatively charged. This was intended to mimic the situation in the intact protein, in which the N-termini of the TM helices would not be charged as they are preceded by 34 extramembraneous residues. Thus, the sequence of each helix of the bundle was: H_2N-Phe^{35}-Cys-Leu-Ile-Leu-Ile-Cys-Leu-Leu-Leu-Ile-Cys-Ile-Ile-Val-Met-Leu-Leu^{52}-CO_2^-

The pore was solvated and MD simulations performed using protocols based on those described

previously [4,5]. The water model employed was a TIP3P three-site model [25] with partial charges $q_O = -0.834$ and $q_H = +0.417$, modified as in the CHARMm parameter set to allow internal flexibility of the water molecules. Model pores were solvated using a pre-equilibrated cylinder (length = 60 Å, radius = 7 Å) of water molecules. Water molecules from this cylinder were selected so that the central pore and the cap regions at either mouth of the pore were solvated, but such that no water molecules were present on the bilayer-exposed surfaces of the pores.

The solvated model pore was energy minimized prior to the MD simulation. A four-stage energy minimization was performed: (a) 1000 cycles of adopted basis Newton Raphson (ABNR) minimization with the protein atoms fixed; (b) 1000 cycles of ABNR with the protein backbone atoms restrained; (c) 1000 cycles of ABNR with weak restraints on the protein Cα atoms only; and (d) 1000 cycles of ABNR with no positional restraints.

During the MD simulation a number of restraints were applied: (a) a cylindrical restraining potential on the waters (see Refs. [4,5] for details) so as to prevent 'evaporation' from the mouths of the pore; (b) *intra*-helix restraints (between NH and CO groups, see Refs. [4,5]) to maintain the TM segments in an α-helical conformation; (c) *inter*-helix restraints (between the geometrical centres of adjacent helices in the bundle) to hold together the helix bundle (see Refs. [26,27]); and (d) a 'bilayer' potential, based on residue-by-residue hydrophobicities [28] to mimic the embedding of the helix bundle in a membrane. Trial simulations with different combinations of these restraints indicated that they prevented the pore model from drifting from the initial model, but did not substantially alter the behaviour of the water molecules either within or at the mouths of the pore.

MD simulations used a 1 fs timestep. The system was heated from 0 to 300 K in 6 ps (5 K, 0.1 ps steps) and equilibrated for 9 ps at 300 K by rescaling of atomic velocities every 0.1 ps. The production stage of the simulation was for 485 ps, giving a total simulation time of 500 ps. The trajectory was analyzed using coordinate sets saved every 1 ps during the production stage of the simulations. Non-bonded interactions (both electrostatic and van der Waals) between distant atoms were truncated using a shift function [22] with a cutoff of 13.0 Å, and a fixed dielectric of $\varepsilon = 1$ was used for electrostatic interactions.

2.3. MD simulations with an ion in the pore

Short MD simulations with a K^+ ion restrained to lie in successive xy-planes along the pore (z) axis were performed in order to evaluate the effect of an ion on the behaviour of the water molecules. For step i the K^+ ion was placed at $(0, 0, z_i)$ and subjected to a quadratic planar restraint with a force constant of 10 kcal mol^{-1} Å^{-2}. The system was subjected to 1000 steps of ABNR energy minimization (to relax any bad contacts between water and ion) followed by 6 ps heating and 9 ps equilibration MD (see above). This process was repeated for the ion at $z_i = -15$ to $+15$ Å in 1-Å steps. Two sets of simulations were preformed: (a) starting with the pore plus water configuration at the end of energy minimization (in the absence of the ion); and (b) starting with the pore plus water configuration at the end the 500 ps MD run. No significant differences in the ion–pore–water interaction energies were observed between these two simulations. The results described below refer to simulation (b). With the K^+ ion restrained at $z = 0$ Å a 100 ps simulation was also performed.

Potential energies of interaction energies of the ion with the pore and/or water were calculated as: (a) $\Delta E_{K,PW} = E(\text{pore + water + } K^+) - E(\text{pore + water}) - E(K^+)$; (b) $\Delta E_{K,P} = E(\text{pore + } K^+) - E(\text{pore}) - E(K^+)$; and (c) $\Delta E_{K,W} = E(\text{water + } K^+) - E(\text{water}) - E(K^+)$. It should be stressed that these are potential energies and so do not take account of entropic contributions to the ion–pore water free energy. Similar simulations were performed with a Cl^- ion instead of the K^+ ion.

2.4. Analysis

Two parameters characterising the dynamic behaviour of water molecules were estimated: the self-diffusion coefficient, D (which measures translational mobility), and the rotational reorientation rate time, τ^{-1} (see Ref. [4] for methodological details). Water dipole orientations were analyzed from coor-

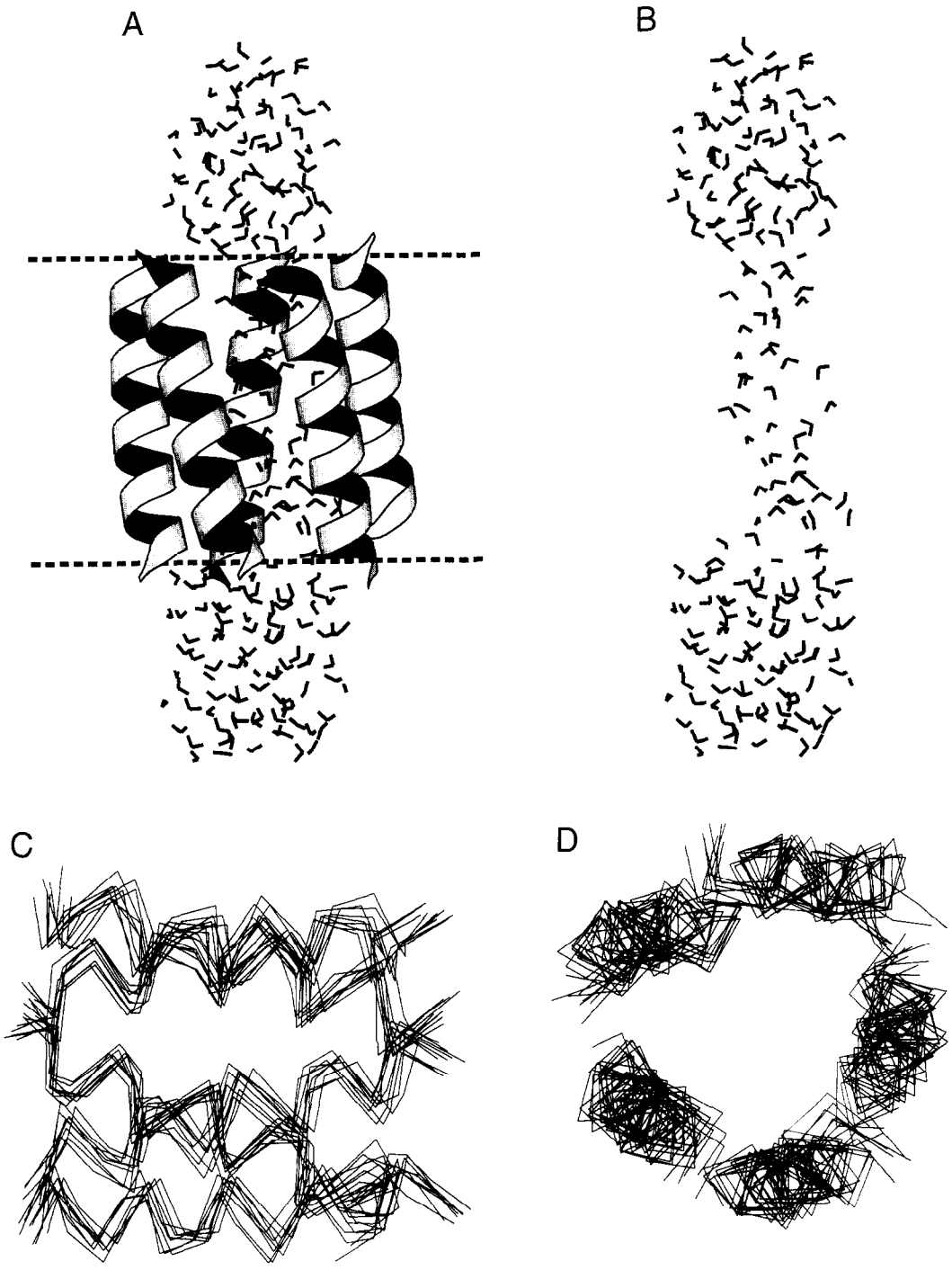

Fig. 1. Structure of the phospholamban pore plus water. (A) The five helices which form the pore are shown in 'ribbons' format, with the water molecules as V-shapes. The limits ($z = \pm 12$ Å) of the bilayer potential are indicated as two broken horizontal lines. (B) Shows just the waters from A. Both diagrams are of the structure midway through the MD simulation, i.e., at $t = 250$ ps. (C) and (D) show Cα traces of the helix bundle at $t = 100$, 150, 200, 250, 300, 350, 400, 450 and 500 ps superimposed. (C) is viewed perpendicular to the pore (z) axis, with the N-termini of the helices on the left-hand side. (D) is viewed down the pore axis.

dinate sets saved at 100 ps and every subsequent 50 ps. The orientation of water molecules relative to the pore (z) axis was measured in terms of the projection onto the z axis of the dipole moment of each water, μ_z, where the pore axis (z) runs from the N-termini to the C-termini of the helices. Thus, a water molecule with its O atom closer to the N-termini and its H atoms closer to the C-termini would have a positive value for μ_z. Thus an undistorted TIP3P water molecule with its dipole exactly parallel to the z axis would have $\mu_z = +2.35$ Debye.

Pore radius profiles were determined using HOLE [29], which gives the pore radius, $r(z)$, as a function of distance along the pore (z) axis. HOLE was also used to calculate predicted conductances for the channel [30]. The pore radius profile was converted to the cross-sectional area of the pore as a function of z: $A(z)$. If the resistivity, ρ, of the electrolyte within the pore were equal to that of the bulk solution the conductance of the structure would be approximately [31,32]:

$$G_{\mathrm{UPPER}} = \left[\int \frac{\rho}{\pi r^2} \mathrm{d}z \right]^{-1}$$

In practice it is found for all the channel structures examined that the experimental conductance is ca. 5 × less than this. Thus, an empirically-based correction function may be introduced, and a reasonable prediction for the conductance obtained from:

$$G_{\mathrm{PRED}} = \frac{G_{\mathrm{UPPER}}}{C(R_{\mathrm{MIN}})}$$

where the correction function, C, depends on the minimum radius, R_{MIN}, of the channel, and ranges in value from ca. 5.6 for $R_{\mathrm{MIN}} = 1.3$ Å (gramicidin A) to ca. 5 for $R_{\mathrm{MIN}} = 4.0$ Å (porin OmpF) [30]. This correction factor takes into the account the differences between an essentially macroscopic description of conductance, as given above, and a truly atomistic description of the microscopic process, such as may be provided by e.g., free energy perturbation calculations [33]. In trials for six experimentally determined channel structures the predictions were accurate to within an average factor of 1.6 to the true value. If there is agreement between the predicted value and the experimentally determined conductance this provides support for the validity of the model.

3. Results

3.1. MD simulation of a solvated phospholamban pore

The pore model which formed the basis of the MD simulation is shown in Fig. 1A,B. This is a snapshot of the system midway through the MD simulation. The left-hand supercoiled helix bundle present in the original model pore (i.e., 1PSL; [10,11]) is retained throughout the solvated MD simulation. A column of water molecules, on average 3 or 4 water molecules in width, extends throughout the length of the pore, widening towards either mouth of the pore. The free C-termini of the helices result in the C-terminal mouth to the pore being encircled a ring of negative charges. This may be compared with e.g., the rings of acidic sidechains at either mouth of the pore of the nicotinic acetylcholine receptor [7,34,35].

From consecutive snapshots (every 50 ps) of the Cα traces of the helices (Fig. 1C,D) it is evident that the fluctuations of the helices do not result in large changes in the bundle geometry relative to the initial model. The RMSD (on Cα atoms only) from the start to the end of the 500 ps simulation was 1.6 Å. In part this is explained by a small degree of 'expansion' of the pore following MD simulation in the presence of water. Thus, in the initial model (1PSL) the mean helix–helix distance for neighbouring pairs of helices was 9.8 (±0.1) Å, whereas the corresponding average across the 500 ps MD simulation was 10.5 (±0.4) Å. A similar expansion upon solvation has been seen in a number of comparable simulations e.g., Ref. [36]. However, it did not alter the overall bundle geometry. For example, the left-handed supercoil does not switch to a right-handed form in the presence of water molecules, in contrast to the situation observed with some other pore models [37]. In the initial model (i.e., 1PSL) the helix–helix crossing angle averaged across adjacent helix pairs of the bundle was $\Omega = +21$ (±2)°, compared with a value for the structure after 500 ps of MD with solvent present of $\Omega = +21$ (±6)°, confirming that substantial in helix bundle geometry had not taken place. Analysis of polypeptide backbone tor-

sion angles revealed that significant changes in intra-helix geometry did not occur. Thus, for the initial model $\langle\phi\rangle = -61\ (\pm 7)^\circ$ and $\langle\psi\rangle = -42\ (\pm 7)^\circ$, whereas at the end of 500 ps of MD, $\langle\phi\rangle = -62\ (\pm 17)^\circ$ and $\langle\psi\rangle = -40\ (\pm 16)^\circ$. The only noticeable helix distortion occurred at the C-terminus of one helix within the bundle. This took place early in the simulation (ca. 10 ps) and was retained for the remainder of the run.

In addition to analysis of the changes in bundle geometry during the MD simulation, it is informative to examine the nature of the pore-lining sidechains. This was achieved by visual inspection map of the inner surface of the pore. Comparison of the initial model, 1PSL, with structures saved at 100 ps intervals during the MD simulation revealed that although fluctuations occurred at the two mouths of the pore, the sidechains which line the central segment of the pore were conserved. Thus the pore lining is dominated by the following sidechains: Cys-36, Ile-40, Leu-43, Ile-47, and Met-50, and remains so throughout the duration of the simulation.

An overview of the conformational dynamics of the pore-lining sidechains was provided by examination of the sidechain torsion angle distributions over the duration of the MD simulation. Overall, this analysis (data not shown) revealed that the sidechain χ_1 angle distributions did not shift significantly from the starting model upon solvation and prolonged MD simulation. In particular the small changes in helix packing during solvation and MD simulation did not result in a major shift in sidechain conformations.

3.2. Water dynamics and orientation within the pore

Analysis of the dynamic behaviour of water molecules within and at the mouths of the pore followed that in our earlier studies of simple pore models [4], focusing on self-diffusion coefficients and rotational reorientation rates of water molecules

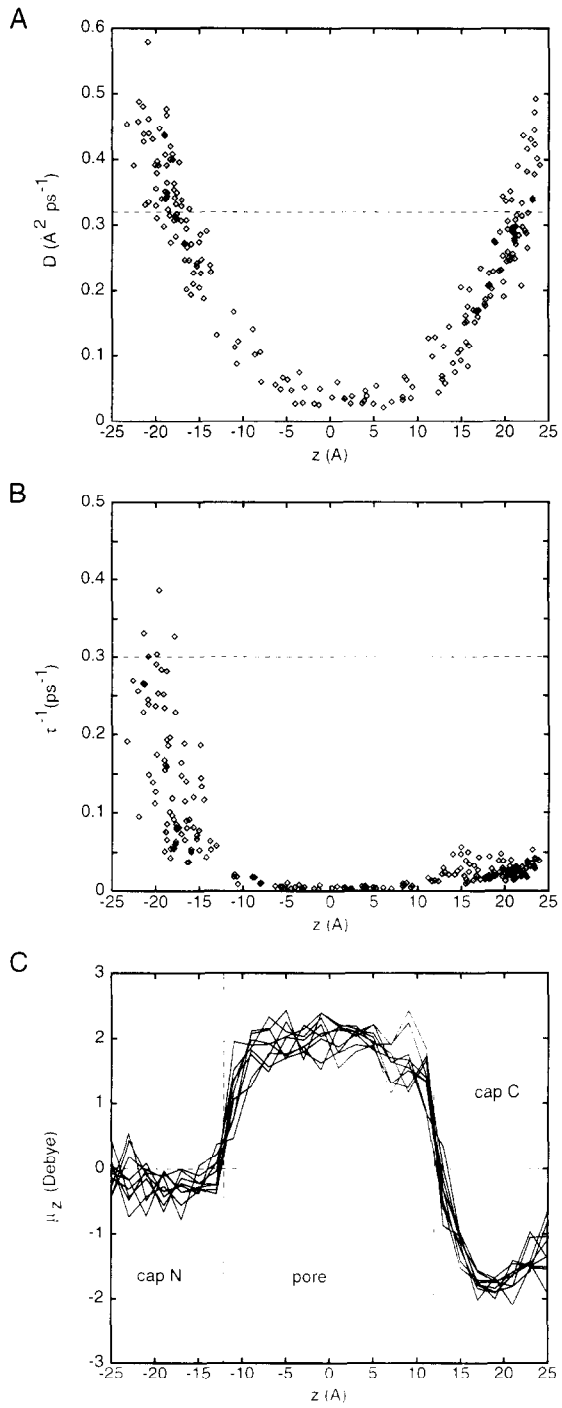

Fig. 2. Analysis of dynamics and orientation of waters. (A) The self-diffusion coefficient (D) of each water molecule is plotted as a function of its average oxygen z coordinate. (B) The water dipole reorientation rate (τ^{-1}) of each water molecule is plotted as a function of its average oxygen z coordinate. In both graphs the horizontal broken line is the corresponding value of the parameter for a bulk TIP3P water simulation. (C) Water dipole orientation profiles. The lines represent μ_z for the water molecules, averaged in 2 Å blocks along the z axis. The superimposed lines correspond to profiles for structures at $t = 100$, 150, 200, 250, 300, 350, 400, 450 and 500 ps.

as functions of their average position along the pore (i.e., z) axis during the simulation. Of course, some water molecules do move along the pore axis, switching between the cap zones and the pore, but the majority remain in one zone, and thus such z-averaging does not blur the dynamics profiles too much. Self-diffusion coefficients (D) of the water molecules are shown in Fig. 2A, where they may be compared with the mean self-diffusion coefficient for the TIP3P water model simulated under 'bulk' conditions [4]. Within the pore (-12 Å $< z < +12$ Å), D is significantly lower than in the caps or than the bulk value. Indeed, within the central section of the pore (-6 Å $< z < +6$ Å) $< D > = 0.04$ (± 0.01) Å^2 ps^{-1}, i.e., almost an order of magnitude lower than the self-diffusion coefficient of bulk TIP3P water (0.32 Å^2 ps^{-1}).

A slightly more complex profile is seen for the rotational relaxation rates (Fig. 2B). Thus, at the N-terminal cap, τ^{-1} is 0.14 (± 0.09) ps^{-1}, i.e., close to the value for bulk water (0.3 ps^{-1}). Within the pore, τ^{-1} falls to 0.008 (± 0.005) ps^{-1}, and then rises to 0.03 (± 0.01) ps^{-1} at the C-terminal mouth. Thus rotational mobility within the pore is reduced by a factor of ca. 40 relative to the bulk. The rotational mobility of the water is also reduced in the vicinity of the C-terminal mouth which, it should be remembered, is encircled by a ring of five negative charges. As will be seen, this reduction of the rotational mobility of the water molecules is matched by alignment of their dipoles relative to the pore axis.

The orientation of the water molecules was probed by calculating the pore axis projections of their dipole moment. In Fig. 2C these dipole projections are plotted as a function of the average position of the water molecule along the pore axis. In the N-terminal cap the water molecules are more or less randomly oriented, with a mean value (average over 100 to 500 ps) for the projected dipole moment of $\langle \mu_z \rangle = -0.21$ (± 0.10) Debye. Within the pore the water dipoles are aligned such that their H atoms point towards the C-terminal mouth of the pore and their O atoms towards the N-terminal mouth, giving $\langle \mu_z \rangle = +1.75$ (± 0.11) Debye. In the C-terminal cap the waters point in the opposite direction, such that $\langle \mu_z \rangle = -1.33$ (± 0.10) Debye. When interpreting these values it should be remembered that the dipole moment of the TIP3P water is 2.35 Debye. Thus the combination of the macrodipoles of the helix backbones and the ring of negative charges at the C-terminal mouth generates significant ordering of the waters both within the pore and at the C-terminal mouth.

The energetics of protein–protein and pore–water interactions within the phospholamban TM helix bundle at the end of the MD simulations yielded the following results: $\Delta E^{\mathrm{VDW}}_{\mathrm{PORE-WATER}} = -150$ kcal mol^{-1} and $\Delta E^{\mathrm{ELEC}}_{\mathrm{PORE-WATER}} = -898$ kcal mol^{-1}, where these are respectively the van der Waals and electrostatic components of the pore–water interaction energy; and $\Delta E^{\mathrm{VDW}}_{\mathrm{HELIX-HELIX}} = -459$ kcal mol^{-1} and $\Delta E^{\mathrm{ELEC}}_{\mathrm{HELIX-HELIX}} = +2262$ kcal mol^{-1}, where these are the van der Waals and electrostatic components of the helix–helix interaction energy for the bundle 'subunits'. Note therefore that the favourable electrostatic interactions of the water dipoles with the helix dipoles to some extent counteract the mutual repulsion of the parallel (and negatively charged) adjacent TM helices.

3.3. A K^+ vs. a Cl^- ion within the pore

To determine whether a hydrophobic helix bundle could provide an energetically favourable permeation pathway for ions, two further series of MD simulations were performed in which a K^+ or a Cl^- ion was translated along the pore. Thus, K^+ ion was placed at successive positions along z, and then 1000 cycles of ABNR energy minimization followed by 15 ps of MD (i.e., 6 ps heating plus 9 ps equilibration) were performed. This was repeated, moving the K^+ ion in 1-Å steps along the pore axis from $z = -15$ Å to $+15$ Å. Preliminary simulations had indicated that 15 ps of MD were sufficient for the water molecules to 'relax' in the electrostatic field around the K^+ ion. Examination of the z-axis projections of the water dipoles at the end of the 15 ps simulations for successive positions of the ion revealed a 'wave' of *local* realignment of the water dipoles tracking the ion along the pore. More detailed analysis (not shown) indicated that about four water molecules are involved in this local realignment.

In order to examine the energetics of pore–water–ion interactions the interaction potential energy profiles of the K^+ ion with (pore + water), of

the ion with the pore, and of the ion with the water were analyzed (Fig. 3A). The $\Delta E_{K/PW}$ profile is relatively flat in the N-terminal half of the pore, with no pronounced barrier as the ion enters the N-terminal mouth. Examination of the two components of this interaction suggest that the unfavourable interaction of the cation with the N-terminal helix dipoles is counteracted by a more favourable interaction with the aligned water dipoles as the ion enters the pore. At the C-terminal mouth there is a highly favourable interaction of the ion with the pore. However, this is balanced to some extent by weakened ion–water

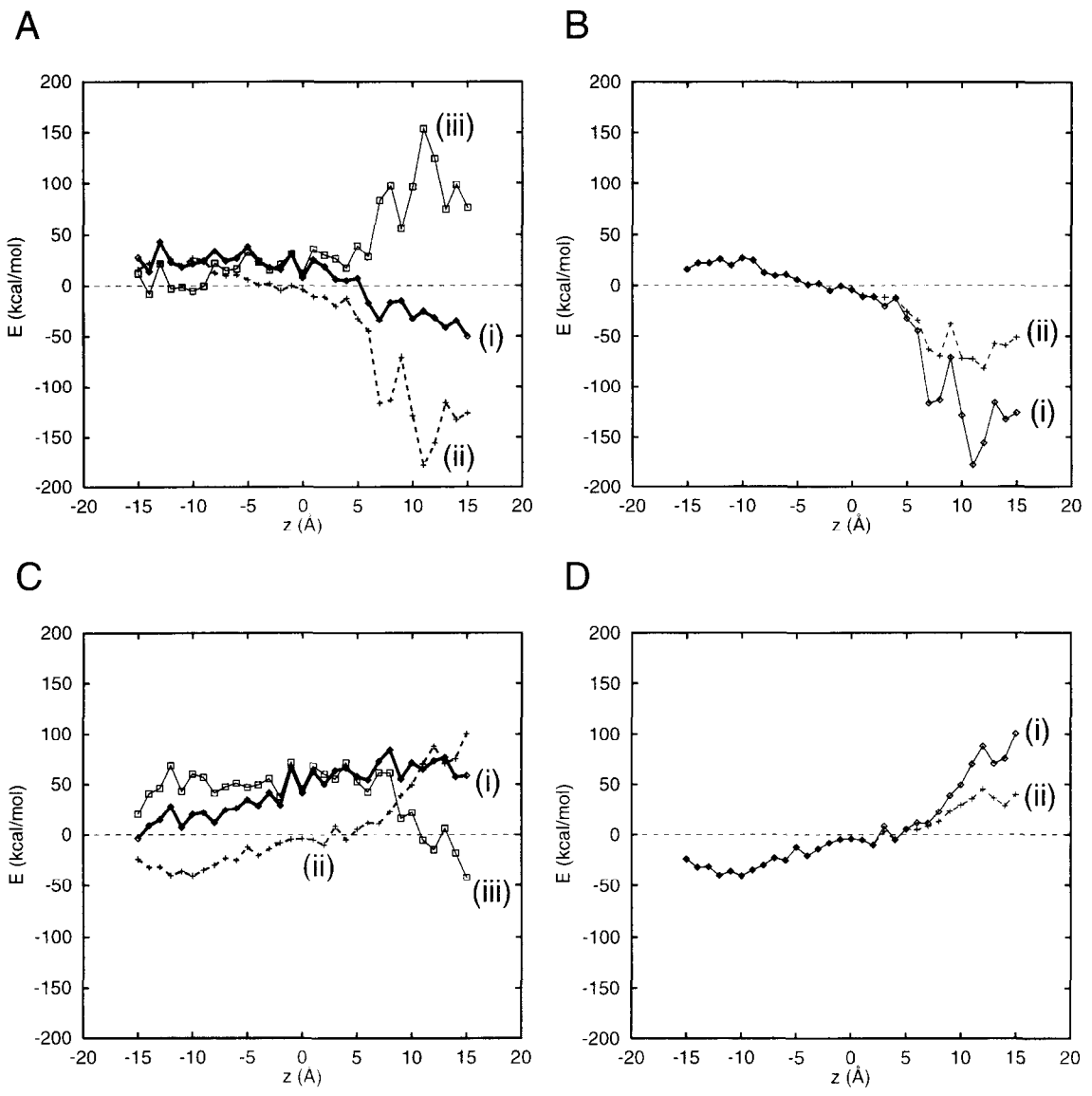

Fig. 3. Interaction energies of ions as a function of their position on z. The interaction energy profiles are shown for a K^+ ion (A) and for a Cl^- ion (C). In each case the three lines correspond to: (i) the ion–(pore + water); (ii) ion–pore; and (iii) ion–water interaction energies for each structure after 15 ps of MD. The ion–(pore + water) and ion–water interaction energies have been normalized by subtraction of the mean potential energy of the corresponding ion simulated in a box of 3375 water molecules. In (B) and (D) the ion–pore interaction energy profiles obtained by including (i) and excluding (ii) the effects of the five negative charges at the C-terminal mouth of the pore are compared, for a K^+ ion (B) and for a Cl^- ion (D).

interactions. Thus the water screens the strong cation–carboxylate ring interactions to an extent. However, the overall K^+ ion–(water + pore) interaction at the C-terminal mouth remains favourable, consistent with the cation selectivity of the phospholamban channel.

An exactly comparable set of simulations were performed using a Cl^- ion instead of a K^+ ion. As for the K^+ ion, the presence of a Cl^- ion within the pore resulted in only local realignment of the water dipoles. More interesting were the interaction energy profiles for the Cl^- ion as it was translated along the pore (Fig. 3C). As expected, the Cl^-–pore profile showed a well at the N-terminal mouth and a barrier (of height ca. 100 kcal mol^{-1}) at the C-terminal mouth of the pore. This barrier was to some extent compensated for by more favourable Cl^-–water interactions at the C-terminal mouth. However, the overall Cl^- ion–(water + pore) interaction energy profile presents a barrier to Cl^- permeation along the entire length of the pore, rising from ca. 20 kcal mol^{-1} at the N-terminal mouth to ca. 60 kcal mol^{-1} at the C-terminal mouth. This reinforces the suggestion that the current model can explain the observed selectivity of channels formed by phospholamban for cations rather than anions.

To dissect further the components of the interaction potential energy profiles, the profiles were recalculated, from the same simulations, but neglecting the contribution of the five negative charges at the C-termini of the helices. The resultant ion–pore profiles are shown in Fig. 3B (for K^+) and Fig. 3D (for Cl^-). In both cases it is evident that the interaction of the ion with the five negative charges makes a significant contribution to the energy profile. Thus, to some extent the ion selectivity of the phospholamban channel will depend on the ionization state of the C-termini of the helices, which in turn may depend on the local micro-environment of these termini in terms of possible counterions. A full analysis of these effects will be the subject of further, rather more elaborate, simulations than are described in the current study.

3.4. Pore radius profile and estimated conductance

As described above, analysis of the pore radius profile may be used to obtain a prediction of channel conductance [30], thus allowing comparison of the model vs. experimental data. Furthermore, although the fluctuations in helix bundle geometry during the course of the MD simulation were relatively small, it was of interest to determine whether these fluctuations had a significant effect on the predicted conductance. Pore radius profiles were analyzed for structures saved every 50 ps during the simulation and compared with the profile for the initial, i.e., IPSL, model (Fig. 4). The limited expansion of the helix bundle upon solvation results in an increase in the pore radius of ca. 0.5 Å averaged along the length of the pore. Overall, the profile after solvation is rather flat, with a mean radius of ca. 2.5 Å, apart from a narrowing of the pore at the C-terminal mouth. Fluctuations in radius at the C-terminal mouth may be linked to fluctuations in backbone conformation of the C-terminus of one of the helices (see above). The pore radius profiles may be used as the basis of estimations of the conductance of the pore. The predicted values of the pore conductance in 200 mM KCl varies range between ca. 50 and 70 ps (see Table 1), whereas the experimentally determined pore conductance with the same electrolyte is ca. 100 ps (S. Smith, personal communication; also see Ref. [8]), i.e., the predicted pore conductance is about half

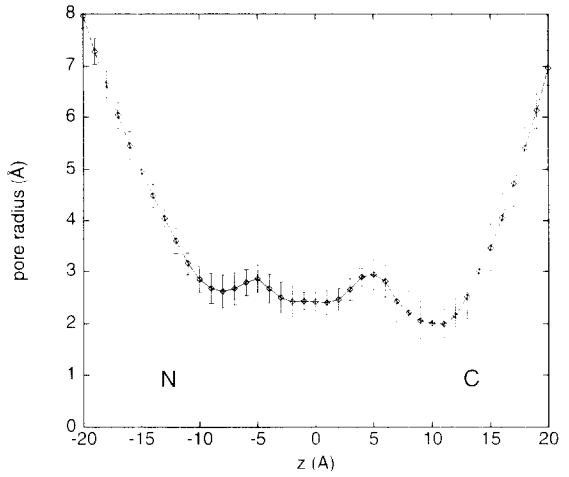

Fig. 4. Pore radius profiles, calculated using HOLE [29]. The broken line is the radius profile for the initial model IPSL. The solid line shows the average (±standard deviation) of the radius profiles for $t = 100$, 150, 200, 250, 300, 350, 400, 450 and 500 ps. In both cases the pore radius is displayed as a function of the position along the z (i.e., pore) axis.

Table 1
Conductance of pore

t (ps)	$\langle R \rangle$ (Å)	G_{UPPER} (ps)	$G_{PREDICT}$ (ps)
100	2.5 (±0.4)	366	69
150	2.6 (±0.5)	280	54
200	2.7 (±0.4)	267	51
250	2.6 (±0.4)	263	50
300	2.8 (±0.5)	304	57
350	2.6 (±0.4)	287	51
400	2.6 (±0.5)	395	72
450	2.4 (±0.4)	265	50
500	2.4 (±0.5)	280	51

The pore radius profile was evaluated for structures at time t during the MD simulation (see Fig. 4), yielding an average (over -12 Å $< z < +12$ Å) radius $\langle R \rangle$.
Conductances were calculated using a resistivity of $\rho = 0.417$ Ωm for 200 mM KCl.

the experimental value. This is within the error limits of the prediction method [30]. In this prediction method an empirical correction factor is derived which indicates that the 'effective resistivity' within the pore is 5 × that of the corresponding bulk solution. A possible explanation for this increased resistivity lies in the perturbed dynamics of water molecules within the pore, as discussed above.

Approximate estimates of pore conductances for equivalent tetrameric and hexameric helix bundles may be obtained, combining the results of previous calculations on pore radii for helix bundles of different stoichiometries [26] with the pore estimate for the pentameric model. Such calculations yield a conductance of ca. 7 to 14 ps for a tetrameric helix bundle, and of 100 to 125 ps for a hexameric helix bundle. Thus, a tetrameric helix bundle is clearly not compatible with the experimental conductance, but a hexameric helix bundle provides a possible alternative to the pentameric model. To distinguish between the pentameric and hexameric alternatives, further experimental data and/or more refined conductance calculations will be required.

4. Discussion

4.1. Methodology

The results of an MD simulation are dependent upon the initial model. In the current study this is not an X-ray structure, but is a plausible model based on a variety of less direct structural data, and so MD simulations on the basis of it are justified. In particular, this model is supported by CD and FTIR data for the secondary structure of the TM segments, by FTIR-ATR data for the transmembrane orientation of the helices, and by mutagenesis, computational and SH/SD exchange data for the orientation of the helices within the bundle [9–11,16]. What is less certain is the number of helices in a bundle. A pentameric helix bundle is supported by computational studies of helix packing interactions [10], and also by the conductance calculations reported in this paper (see below). Furthermore, a pentameric coiled-coil model has been proposed, independently, by Simmerman et al. [17] on the basis of SDS-PAGE analysis of the oligomeric state of wild type and of mutated channel-forming domains of phospholamban. However, it has also been suggested that there may exist, within the bilayer, a dynamic equilibrium of oligomeric states [19].

The MD simulations with water molecules are similar to those in previous studies of simple channel models and channel-forming peptides [4,5], and in studies of water within the pores of gramicidin A [2,38] and cyclic peptide nanotubes [3]. In the case of gramicidin A, where more experimental data are available, such simulations have yielded e.g., water self-diffusion coefficients which are in good agreement with the experimental values [2]. It is therefore reasonable to assume that this procedure yields physically meaningful results. However, it is important to consider possible limitations of the simulations. The first of these is the relative simplicity of the force field, and particularly of the water model employed. The use of a point charge model, which does not allow for electronic polarizability, may mean that some the water properties do not agree exactly with experimental values, even in bulk state simulations [39]. This may be exacerbated by, e.g., the use of distance cutoffs in calculation of long range electrostatic interactions.

It is also useful to consider the possible effects of the restraints imposed during the simulation. For water molecules these consisted of a restraining cavity of cylindrical geometry lying outside the pore formed by the protein. Thus, within the pore water molecules never experience the restraining cavity

potential. At either cap of the pore, water molecules experience a restraining potential which prevents their evaporation from the system. Previous simulations [40] have shown that such a cavity potential does not substantially modify the dynamic behaviour of the waters in the caps. Two classes of restraint were applied to the phospholamban helices. Intra-helix distance restraints were used to maintain the α-helical geometry. Previous simulations [4] on bundles of Ala_{20} helices have shown that such restraints do not seem to influence the behaviour of the water. Inter-helix restraints have also been evaluated in a number of previous simulations [4,27], in which they did not effect the packing of the helices. For example, despite such restraints quite substantial changes in helix crossing angle may occur [27,37]. The empirical membrane-mimicking potential applied to the sidechains has been employed in a number of simulations, both of single helices interacting with a bilayer [28] and of the helix bundle of bacteriorhodopsin [41]. The main effect of this potential is to keep the phospholamban helices 'in register' along the z-axis. Simulations without this potential gave similar results both in terms of the geometry of the helix bundle and the dynamic properties of the water molecules.

The major omission from our simulations is that an explicit bilayer is not present. Inclusion of this would lead to a considerable increase in cpu time, and may not be justified at this stage. However, as the direct interactions of the water molecules are with one another and with the protein atoms lining the pore, omission of a lipid bilayer is an acceptable first approximation. A similar approach has been used by [6] in simulation studies of the pore domain of a Na^+ channel. The other omission from the model is the 34 residues from the N-terminus of each phospholamban molecule. This is not too serious, as the TM helix alone can self-assemble in a lipid bilayer to form cation permeable channels [8]. However, there are differences between the conductance properties of the channels formed by the intact protein and those formed by the C-terminal fragment, and so it may be necessary in the future to extend the MD simulations to a more complete model of the channel, as discussed in [11].

A methodological aspect which merits discussion is the simulation of interactions of a K^+ vs. a Cl^- ion with the (pore + water). The xy-plane restraints placed upon the ion were such that it could deviate from the plane by ca. ± 0.5 Å for each value of z. Restricting the duration of the simulation to 15 ps heating + equilibration was sufficient to allow the waters to 'relax' about the ion, as shown by comparison with the 100 ps simulation with either a K^+ or a Cl^- ion at $z = 0$. Two sets of K^+ ion simulations, with different starting configurations of the waters, yielded much the same results. Furthermore, studies on related channels formed by helix bundles suggest that simulations in which the ion is *not* returned to $x = y = 0$ Å at the beginning of each step along z do not yield significantly different profiles (Bull and Sansom, unpublished data). Thus, it seems that the potential energy profiles are not over-sensitive to the initial arrangement of the water molecules within the pore. However, it must be stressed that the profiles are of potential energies of interaction, and do not take account changes in the entropy of the system as the ion is moved along the channel.

The HOLE method for determination of pore radius profiles has been discussed fully in a number of papers [26,29]. The use of HOLE-derived pore radius profiles to estimate channel conductances is somewhat newer [30–32], and merits some discussion. It is based upon the assumption that the resistance of a channel may be calculated as the sum of the resistances of a series of concentric cylindrical discs along the channel, plus an access resistance [1] at either mouth. This assumption is a reasonable approximation provided that the channel does not deviate too greatly from a regular cylindrical geometry. This is the case for the phospholamban channel. By assuming that the transbilayer pore is filled with an electrolyte of identical resistivity to that of the external bulk solutions one obtains an upper limit to the conductance of the pore. It has been shown, by comparison with channels of known three dimensional structure *and* conductance (e.g., gramicidin A, porins), that the upper limit on the conductance is about five times larger than the experimental value. Thus, an empirical scaling factor of ca. $0.2\times$ should be applied in order to arrive at a predicted conductance [30]. This scale factor may include two effects which increase the effective resistivity within the pore. The first is a reduction in diffusion rates of water molecules (and hence, one assumes, of hy-

drated ions) within the pore. The second is the presence of energy barriers to the passage of an ion due to, for example, the presence of charged or polar residues lining the channel. Indeed, a good fit to the temperature behaviour of the conductivity of sodium and potassium channels has been obtained by combining a simple expression for G_{UPPER} (based on an assumed pore geometry) with a simple single-barrier model which represents the presence of polar residues within the pore lining [31].

4.2. Biological implications

The simulation results presented in this paper do not address the debate concerning the physiological role of channel formation by phospholamban. Rather, they address the biophysical question of *how* a bundle of TM helices lacking any polar sidechains (other than cysteine) might form a stable ion-permeable pore within a lipid bilayer.

The simulations of the phospholamban TM helix bundle with water molecules within and at either mouth of the pore provide further evidence supporting the IPSL model of [10,11]. Firstly, the structure of the pore does not undergo any profound changes during the 500 ps simulation, suggesting that the in vacuo simulations used to derive the initial model [10] had identified a particularly stable mode of packing of the transmembrane helices. Secondly, the predicted pore conductance agrees, within a factor of two, with the experimental estimate of the conductance. This provides strong evidence in favour of a pentameric, rather than a tetrameric, assembly of phospholamban helices. This is a key point for modelling the conductance events and understanding the mechanism of selectivity. There is evidence from SDS-PAGE, particularly of phospholamban chimera, that the protein can exist as both lower and higher order oligomers [9]. One possibility that has not been excluded by the previous structural measurements and modelling studies is that the pentameric complex represents a closed conformation, while a higher order complex, such as a hexamer, represents the open or conducting conformation. The conductance calculations presented in this paper argue that the pentameric complex as modelled by Adams et al. [10] is consistent with an open conformation, although they do not exclude the possibility of channels also being formed by hexameric assemblies.

The alignment of the water dipoles within the phospholamban pore by the helix dipoles has also been observed seen in a number of models of channels made up of parallel helix bundles [4,5]. A simple analysis of the energetics of bundle formation suggests that favourable interactions between the helix dipoles and water dipoles may contribute to the stability of the TM helix bundle. However, more elaborate simulations in the presence of explicit phospholipid molecules will be required to obtain an estimate of the relative contributions of various factors to TM helix bundle stability.

Preliminary analysis of the potential energy profile of a K^+ ion as it is 'dragged' through the phospholamban pore provides further evidence for the importance of water. If one calculated such a profile in vacuo the potential energy barrier at the N-terminal mouth (due to the aligned helix dipoles) and the deep potential well at the C-terminal mouth (due to the ring of negative charges) would seem incompatible with a high conductance cation selective pore. However, the presence of water molecules within the pore flattens this potential profile, in that the aligned water dipoles cancel out the barrier at the N-terminal mouth of the pore, and reduce the depth of the well at the C-terminal mouth. Such flattening of the potential profile by water also occurs for a Cl^- ion translated through the pore. However, the effect of the water molecules is insufficient to entirely compensate for the electrostatic repulsion between the Cl^- ion and the ring of negatively charged termini at the C-terminal mouth of the pore. Thus, the model channel is predicted to be cation selective, in agreement with the experimental data for phospholamban.

In order to extend the use of MD simulations to relate the phospholamban pore model to the physiological properties of the channel, several refinements will be needed. Perhaps the most important refinement will be to establish the high resolution structure of the pore and the dynamics of sidechains that may influence the pore diameter. The structure can be mapped out by internuclear distance constraints obtained using magic angle spinning NMR methods [42] while sidechain dynamics can be established by deuterium NMR of selectively deuterated sites [43]. One of the conclusions of the cysteine sulphydryl exchange studies [16] was that the lack of exchange

of Cys 36 and Cys 46 demonstrated that phospholamban forms a stable channel complex. This contrasts with many other peptide channels that only transiently associate to form a pore.

In terms of the MD simulations per se, the most useful refinements would be inclusion of an explicit model of the lipid bilayer, and a more detailed treatment of the protonation state of the C-terminal carboxylic acid groups. The latter could be achieved by the application of continuum electrostatics calculations [44] to the current model in order to estimate the pK_As of these groups. Preliminary calculations using such methods (Adcock, Smith and Sansom, unpublished data) suggest a significant increase in the pK_A above that for an isolated carboxylic acid group. This would be expected to reduce the size of the potential well for cations (and of the potential barrier for anions) at the C-terminal mouth of the pore.

Acknowledgements

This work was supported by a grant from the Wellcome Trust (to MSPS). Oliver Smart is a Wellcome Trust Research Fellow.

References

[1] B. Hille, Ionic Channels of Excitable Membranes, Sinauer Associates, Sunderland, MA, 1992.
[2] B. Roux, M. Karplus, Ann. Rev. Biophys. Biomol. Struct. 23 (1994) 731.
[3] M. Engels, D. Bashford, M.R. Ghadiri, J. Am. Chem. Soc. 117 (1995) 9151.
[4] J. Breed, R. Sankararamakrishnan, I.D. Kerr, M.S.P. Sansom, Biophys. J. 70 (1996) 1643.
[5] P. Mitton, M.S.P. Sansom, Eur. Biophys. J. 25 (1996) 139.
[6] C. Singh, R. Sankararamakrishnan, S. Subramanian, E. Jakobsson, Biophys. J. 71 (1996) 2276.
[7] R. Sankararamakrishnan, C. Adcock, M.S.P. Sansom, Biophys. J. 71 (1996) 1659.
[8] R.J. Kovacs, M.T. Nelson, H.K.B. Simmerman, L.R. Jones, J. Biol. Chem. 263 (1988) 18364.
[9] I.T. Arkin, P.D. Adams, K.R. MacKenzie, M.A. Lemmon, A.T. Brünger, D.M. Engelman, EMBO J. 13 (1994) 4757.
[10] P.D. Adams, I.T. Arkin, D.M. Engelman, A.T. Brünger, Nature Struct. Biol. 2 (1995) 154.
[11] I.T. Arkin, M. Rothman, C.F.C. Ludlam, S. Aimoto, D.M. Engelman, K.J. Rothschild, S.O. Smith, J. Mol. Biol. 248 (1995) 824.
[12] L.H. Pinto, L.J. Holsinger, R.A. Lamb, Cell 69 (1992) 517.
[13] K.C. Duff, R.H. Ashley, Virology 190 (1992) 485.
[14] M.S.P. Sansom, I.D. Kerr, G.R. Smith, H.S. Son, Virology 233 (1997) 163.
[15] S.O. Smith, R. Jonas, M. Braiman, B.J. Bormann, Biochemistry 33 (1994) 6334.
[16] L.T. Arkin, K.R. MacKenzie, L. Fisher, S. Aimoto, D.M. Engelman, S.O. Smith, Nature Struct. Biol. 3 (1996) 240.
[17] H.K.B. Simmerman, Y.M. Kobayashi, J.M. Autry, L.R. Jones, J. Biol. Chem. 271 (1996) 5941.
[18] H. Masaki, Y. Sato, W.S. Luo, E.G. Kranias, A. Yatani, Am. J. Physiol. 41 (1997) H606.
[19] R.L. Cornea, L.R. Jones, J.M. Autry, D.D. Thomas, Biochemistry 36 (1997) 2960.
[20] Y. Kimura, K. Kurzydlowski, M. Tada, D.H. MacLennan, J. Biol. Chem. 271 (1996) 21726.
[21] G. Hughes, A.P. Starling, R.P. Sharma, J.M. East, A.G. Lee, Biochem. J. 318 (1996) 973.
[22] B.R. Brooks, R.E. Bruccoleri, B.D. Olafson, D.J. States, S. Swaminathan, M. Karplus, J. Comp. Chem. 4 (1983) 187.
[23] P.J. Kraulis, J. Appl. Cryst. 24 (1991) 946.
[24] F. Bernstein, T. Koetzle, G. Williams, E. Meyer, M. Brice, J. Rodgers, O. Kennard, T. Shimanouchi, M. Tasumi, J. Mol. Biol. 112 (1977) 535.
[25] W.L. Jorgensen, J. Chandresekhar, J.D. Madura, R.W. Impey, M.L. Klein, J. Chem. Phys. 79 (1983) 926.
[26] I.D. Kerr, R. Sankararamakrishnan, O.S. Smart, M.S.P. Sansom, Biophys. J. 67 (1994) 1501.
[27] I.D. Kerr, D.G. Doak, R. Sankararamakrishnan, J. Breed, M.S.P. Sansom, Prot. Eng. 9 (1996) 161.
[28] P.C. Biggin, M.S.P. Sansom, Biophys. Chem. 60 (1996) 99.
[29] O.S. Smart, J.M. Goodfellow, B.A. Wallace, Biophys. J. 65 (1993) 2455.
[30] O.S. Smart, J. Breed, G.R. Smith, M.S.P. Sansom, Biophys. J. 72 (1997) 1109.
[31] S. Kuyucak, S.H. Chung, Biophys. Chem. 51 (1994) 15.
[32] M.S.P. Sansom, I.D. Kerr, Biophys. J. 69 (1995) 1334.
[33] B. Roux, M. Karplus, Biophys. J. 59 (1991) 961.
[34] K. Imoto, C. Busch, B. Sakmann, M. Mishina, T. Konno, J. Nakai, H. Buyo, Y. Mori, K. Kukuda, S. Numa, Nature 335 (1988) 645.
[35] D. Bertrand, J.L. Galzi, A. Devillers-Thiéry, S. Bertrand, J.P. Changeux, Curr. Opin. Cell Biol. 5 (1993) 688.
[36] A. Grice, I.D. Kerr, M.S.P. Sansom, FEBS Lett. 405 (1997) 299.
[37] R. Sankararamakrishnan, M.S.P. Sansom, FEBS Lett. 377 (1995) 377.
[38] S.W. Chiu, E. Jakobsson, S. Subramanian, J.A. McCammon, Biophys. J. 60 (1991) 273.
[39] V. Daggett, M. Levitt, Annu. Rev. Biophys. Biomol. Struct. 22 (1993) 353.
[40] M.S.P. Sansom, I.D. Kerr, J. Breed, R. Sankararamakrishnan, Biophys. J. 70 (1996) 693.
[41] F. Jähnig, O. Edholm, J. Mol. Biol. 226 (1992) 837.
[42] S.O. Smith, Curr. Opin. Struct. Biol. 3 (1993) 755.
[43] K.C. Lee, S. Huo, T.A. Cross, Biochemistry 34 (1995) 857.
[44] A. Karshikoff, V. Spassov, S.W. Cowan, R. Ladenstein, T. Schirmer, J. Mol. Biol. 240 (1994) 372.